# Sensorless Speed Control of Nonsalient Permanent-Magnet Synchronous Motor Using Rotor-Position-Tracking PI Controller

Jul-Ki Seok, *Member, IEEE*, Jong-Kun Lee, *Student Member, IEEE*, and Dong-Choon Lee, *Member, IEEE*

***Abstract*—This paper presents a new velocity estimation strategy of a nonsalient permanent-magnet synchronous motor (PMSM) drive without a high-frequency signal injection or special pulsewidth-modulation (PWM) pattern. This approach is based on the $d$-axis current regulator output voltage of the drive system that has the information of rotor position error. Rotor velocity can be estimated through a rotor-position-tracking proportional–integral (PI) controller that controls the position error to zero. For zero and low-speed operation, the PI controller gains of rotor position tracking controller have a variable structure according to the estimated rotor velocity. In order to boost the bandwidth of the PI controller around zero speed, a loop recovery technique is applied to the control system. The proposed method only requires the flux linkage of the permanent magnet and is insensitive to parameter estimation error and variation. The designers can easily determine the possible operating range with a desired bandwidth and perform vector control even at low speeds. The experimental results show the satisfactory operation of the proposed sensorless algorithm under rated load conditions.**

***Index Terms*—$d$-axis current regulator output voltage, nonsalient permanent-magnet synchronous motor (PMSM) drive, rotor-position-tracking proportional–integral (PI) controller, velocity estimation strategy.**

## I. Introduction

THE first generation of sensorless control on a permanent-magnet synchronous motor (PMSM) is based on rotor flux orientation by integration of back electromotive force (EMF) [1]–[3]. These approaches need accurate motor electrical parameters and fail to operate at low and zero speed since the information of back EMF is too low.

Recently, simpler and more effective algorithms have been developed: high frequency injection method and constant frequency pattern method [4], [5]. The high-frequency injection method uses the impedance difference of the motor and can obtain position information even at low and zero speed [4]. The nonsalient PMSM originally has a very small magnetic saliency or $d-q$ axis impedance difference. In order to amplify this small difference, in this study, the magnitude and frequency of the high-frequency voltage signal amount to 100 V and 850 Hz for PMSM with 180 Vrms of the rated voltage. Thus, this may cause undesirable side effects such as large harmonic losses and acoustic noise. The overhead of the injection voltage results in poor utilization of the drive and can be concluded that the high frequency injection method is not completely effective when applied to PMSM without rotor saliency. In addition, the high frequency excitation scheme usually requires a special signal processing technique and also limits the upper operating speed range below a few hundred hertz due to the extraction of injected signal.

In the constant frequency pattern method [5], the speed is estimated by processing output voltages of the $d$-axis synchronous proportional–integral (PI) current regulator in high speed range, and the current with a constant magnitude and a prepatterned frequency is injected from standstill to medium speed range. Open-loop operation is maintained in the low-speed region until a given speed at which the rotor position estimate is sufficiently accurate. The performance of the open loop control is heavily dependent on the selection of reference speed curve and the setting of the ratio of current magnitude to frequency [6]. This selection procedure can be quite tedious in finding the best operating conditions fitting their needs, which may be undesirable in an industrial sense. In addition, it needs an extra transition algorithm between two different control schemes and cannot perform the vector control in the low- and medium-speed region. There is no guideline of the sensorless PI controller gain setup or tuning, which decides position/velocity estimation and closed loop control performance. Thus, it relies too much on the intuition and experience of the designer in order to get the best fit for specific applications.

This paper presents a new velocity estimation strategy of a nonsalient PMSM drive without high frequency signal injection or special pulsewidth-modulation (PWM) pattern. This approach is based on the $d$-axis synchronous current regulator output voltage, which includes the information of rotor position error. The proposed controller utilizes a rotor position tracking PI controller to estimate the rotor velocity, which is used to control the rotor position error to zero. Its dynamic behavior has been characterized by frequency-domain specifications such as phase margin and bandwidth assignment, and analytic tuning formulas for the PI tracking controller are also derived. At very low speed, PI controller gains of the rotor position tracking controller have a variable structure according to the estimated rotor velocity. In order to boost the bandwidth of

Manuscript received June 16, 2004; revised November 17, 2004. Abstract published on the Internet January 25, 2006.

J.-K. Seok and D.-C. Lee are with the School of Electrical Engineering, Yeungnam University, Kyongsan 712-749, Korea (e-mail: doljk@yu.ac.kr; dclee@yu.ac.kr).

J.-K. Lee is with the Robot Institute, Daewoo Ship-Building and Marine Engineering Company Ltd., Geoje City 712-749, Korea (e-mail: ljg1999455@hotmail.com).

Digital Object Identifier 10.1109/TIE.2006.870728

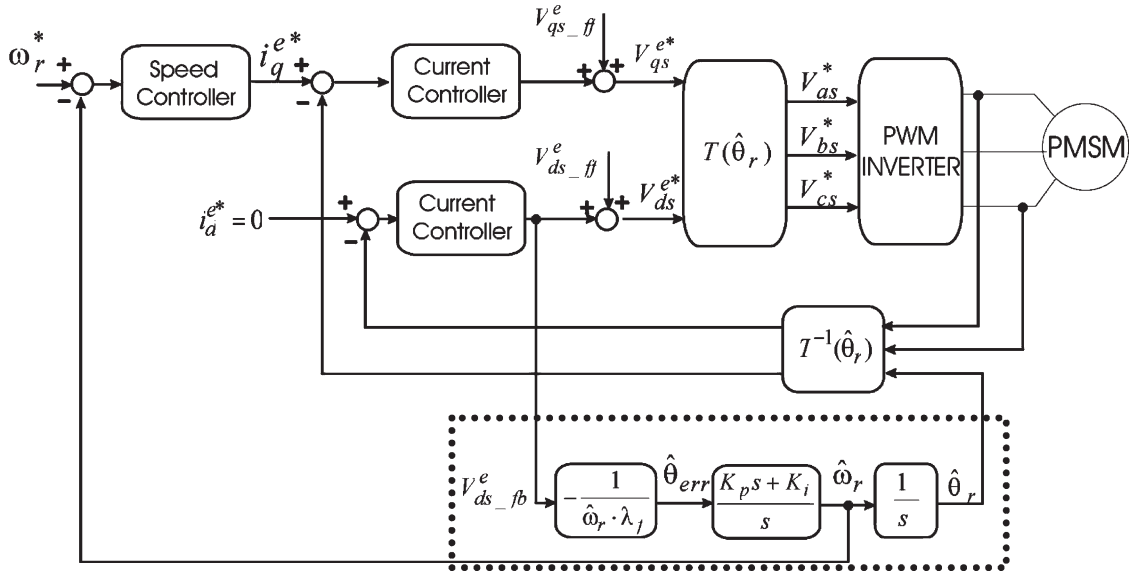


Fig. 1. Overall control structure of the proposed sensorless algorithm.

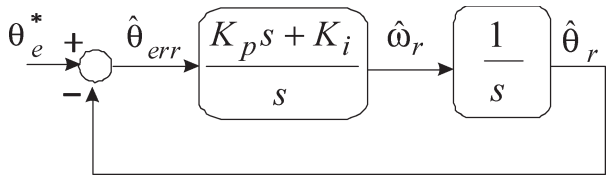

Fig. 2. Block diagram of the sensorless control scheme in Region II.

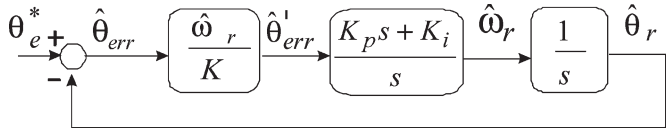

Fig. 3. Block diagram of the sensorless control scheme in Region I.

the PI controller around zero speed, a loop recovery technique is applied to the control system. The proposed sensorless algorithm can provide an accurate description of the control authority to a certain operating range with a desired bandwidth and perform the vector control even at low speeds. The developed algorithm has been implemented on an actual 600-W PMSM drive system to confirm the effectiveness of the proposed scheme.

## II. Analysis of Proposed Sensorless Control in Frequency Domain

The information of rotor position error can be extracted from the $d$-axis synchronous current regulator output voltage [5] $V^e_{ds\_fb}$ as

$$\hat{\theta}_{\rm err} = \frac{-V^e_{ds\_fb}}{\hat{\omega}_r \lambda_f} \tag{1}$$

where $\hat{\theta}_{\rm err}$ is the position error, $\hat{\omega}_r$ indicates the estimated electrical rotor velocity, and $\lambda_f$ is the flux linkage of the permanent magnet. The overall sensorless control block diagram is shown in Fig. 1. Position error can be controlled to zero by the rotor position tracking PI controller. As is clear from (1), in zero and extreme low-speed region ($\hat{\omega}_r \cong 0$), the position error can be amplified, and this may cause instability problems of the tracking PI controller. Thus, an initial starting may fail at standstill, and this control scheme is only available in the high-speed region (Region II). Fig. 2 shows the block diagram of sensorless control scheme in Region II.

To overcome these unwanted starting fails at zero and low speed (Region I), it is desirable that the position error be limited using a constant as

$$\hat{\theta}'_{\rm err} = \frac{\hat{\omega}_r}{{\rm sgn}(\hat{\omega}_r)k}\hat{\theta}_{\rm err} = \frac{V^e_{ds\_fb}}{K\lambda_f} \tag{2}$$

where $K$ indicates a constant value and ${\rm sgn}(\cdot)$ denotes the sign function. If the condition of (2) is considered, the sensorless control block diagram at Region I can be redrawn as shown in Fig. 3.

## III. Tuning Formulas for Rotor Position Tracking PI Controller

The following equation for phase margin $\phi_m$ is obtained from the basic definition of phase margin [7], i.e.,

$$\phi_m = \arg\left[G_c(j\omega_g)G_p(j\omega_g)\right] + \pi \tag{3}$$

where $G_c(s)$ and $G_p(s)$ in Region II are given by

$$G_c(s) = \frac{K_p s + K_i}{s} \tag{4}$$

$$G_p(s) = \frac{1}{s} \tag{5}$$

and the system bandwidth $\omega_g$ is

$$|G_c(j\omega_g)G_p(j\omega_g)| = 1. \tag{6}$$

Substituting (4) and (5) into (3) and (6) gives

$$\omega_g = \sqrt{\frac{K_p^2 + \sqrt{K_p^4 + 4K_i^2}}{2}} \tag{7}$$

$$\phi_m = \arctan\frac{K_p}{K_i}\sqrt{\frac{K_p^2 + \sqrt{K_p^4 + 4K_i^2}}{2}}. \tag{8}$$

Using (7) and (8), solving for PI gains of Region II gives

$$K_p = \omega_g\sqrt{\frac{(\tan\phi_m)^2}{1+(\tan\phi_m)^2}} \tag{9}$$

$$K_i = \omega_g^2\sqrt{\frac{1}{1+(\tan\phi_m)^2}}. \tag{10}$$

Many engineers think directly in terms of $\phi_m$ in judging whether a control system is adequately designed. Practically, a desirable $\phi_m$ is often considered as

$$30^\circ < \phi_m < 60^\circ. \tag{11}$$

However, the system bandwidth is limited by inverter nonlinearities, controller lagging properties, and current measurement errors. Usually, the estimator poles can be chosen to be two or six times faster than controller poles. This is to ensure the faster decay of the estimator error compared with the desired dynamics. As another specification, the bandwidth of the rotor position tracking PI controller should be two or six times higher than the speed controller bandwidth.

Consider the rotor position tracking PI controller in Fig. 3 as

$$G_c(s) = \frac{K_p's + K_i'}{s} \tag{12}$$

where $K_p' = (\hat{\omega}_r/K)K_p$ and $K_i' = (\hat{\omega}_r/K)K_i$.

Therefore, (12) is used to design PI controller gains in Region I. If the estimated velocity increases up to a value of $K$, then gains of Region II are same as those of Region I. This means the proposed sensorless scheme automatically switches the control mode between Regions I and II as the motor speed is varying. For this purpose, $K$ is fixed in Region I and $K = \hat{\omega}_r$ in Region II as shown in Fig. 4.

Hence, from (7), the bandwidth of the rotor position tracking PI controller at zero and low speed can be obtained as

$$\omega_g = \sqrt{\frac{\left(\frac{\hat{\omega}_r(t)}{K}K_p\right)^2 + \sqrt{\left(\frac{\hat{\omega}_r(t)}{K}K_p\right)^4 + 4\left(\frac{\hat{\omega}_r(t)}{K}K_i\right)^2}}{2}}. \tag{13}$$

In (13), it can be seen that the bandwidth of the proposed position tracking PI controller in Region I is varying according to the estimated velocity. In the speed region less than $K$, the rotor position and velocity yield a sluggish dynamics because the varying bandwidth is very low. This result explains that the system is not observable around zero speed in back-EMF-based sensorless methods. To boost the bandwidth at very low speed, a lead compensator is introduced to recover the loop dynamics as shown in Fig. 5. This simple compensator sufficiently improves the dynamic estimation behavior at low speeds in comparison with the initial PI estimator as illustrated in Fig. 6.

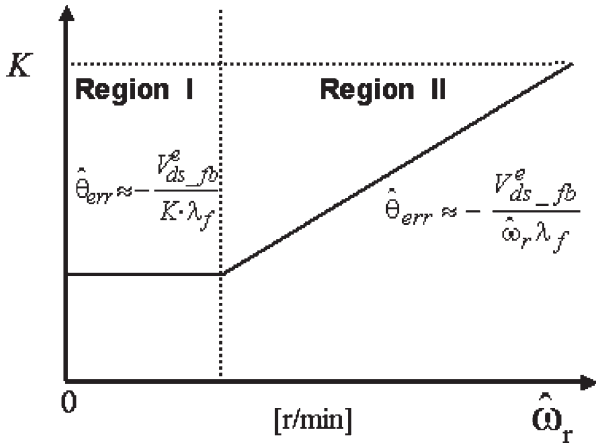


Fig. 4. Trajectory of $K$ for automatic control mode switching.

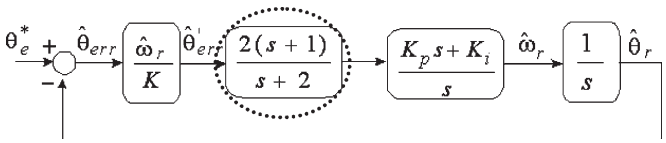


Fig. 5. Block diagram of the sensorless control with lead compensator in the low-speed operation.

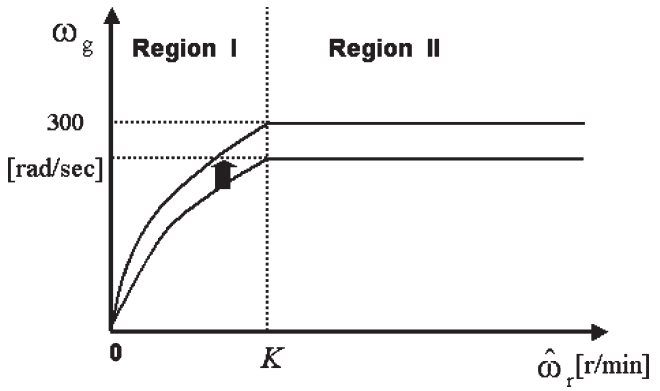


Fig. 6. Bandwidth locus of the proposed PI controller with lead compensator.

Fig. 7 illustrates that a smaller value of $K$ can make the loop bandwidth higher in the low-speed region. For example, if $K$ is 10, the sensorless loop gain will become 300 rad/s at around 30 r/min. Using this result, designers can easily determine the possible operating range with a desired bandwidth before startup and the proposed algorithm enables the vector control over 30 r/min. In industrial fields, one of the most important interests is to capture the dynamics of the control system and to verify that it provides enough control authority at a given operating frequency. From this point of view, it is evident that the proposed sensorless algorithm can provide an accurate description of the control authority to a certain operating range

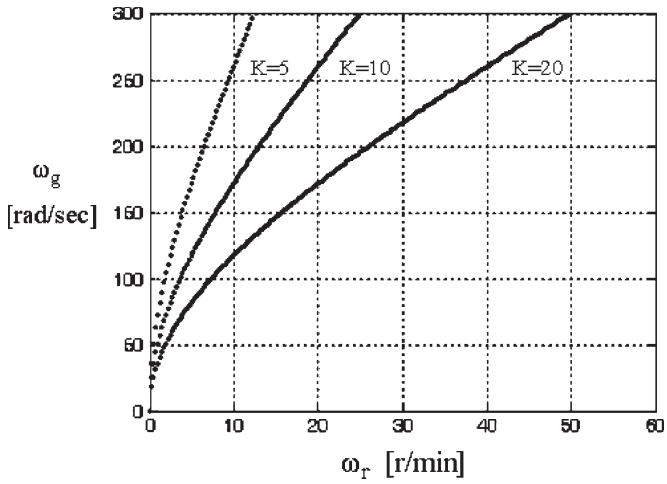


Fig. 7. Bandwidth locus of the proposed PI controller according to rotor velocity.

TABLE I
RATINGS AND KNOWN PARAMETERS OF PMSM UNDER TEST

| 3-Phase, 220[V], 600 [W], 8 Poles | |
|---|---|
| Rated speed | 3000 r/min |
| Torque constant | 0.477 Nt-m/A |
| Moment of inertia | $1.1\times10^{-4}$ Kg-m$^2$ |
| Nominal flux linkage | 0.352 Vrms/rpm |

with a desired bandwidth. This can never be achieved in other back-EMF-based sensorless schemes.

## IV. SIMULATION RESULTS

The proposed sensorless algorithm is tested on a 600-W PMSM in Table I using Matlab/Simulink. From frequency-domain specifications, the phase margin is 50° and $K$ is set to 10, which means that the control mode switching occurs at 25 r/min. Then, bandwidths of the speed controller and the rotor position tracking PI estimator are set to 100 and 300 rad/s, respectively. Sampling periods of the current and speed control loop are 50 $\mu$s and 1 ms, respectively.

Fig. 8 shows the estimated and actual speed with a varying speed command from 0 to 1000 to 500 r/min. The estimated speed properly follows the actual speed in both low-speed and high-speed ranges. It can be seen that the proposed estimation scheme operates well with seamless transition between Regions I and II.

Fig. 9 shows a plot of estimated and measured speed responses with a step speed command while the motor is running from 100 to 50 to 150 r/min. From the top, the speed command, estimated speed, actual speed for monitoring, and $q$-axis current are depicted. In this test, the proposed algorithm does not lose the estimation capability even under low-speed transient change.

Fig. 10 shows the responses of the proposed sensorless scheme with 100 r/min speed command under the half-rated load condition. Speed estimation and control are robust under transient torque change.

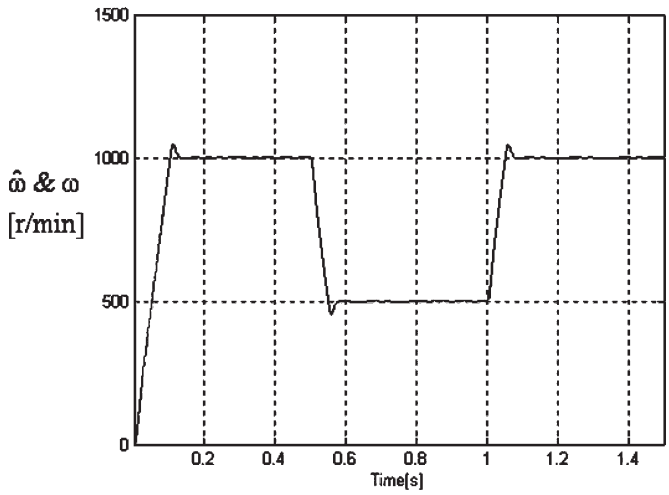


Fig. 8. Estimated and actual rotor speed with varying speed command ($0 \rightarrow 1000 \rightarrow 500$ r/min).

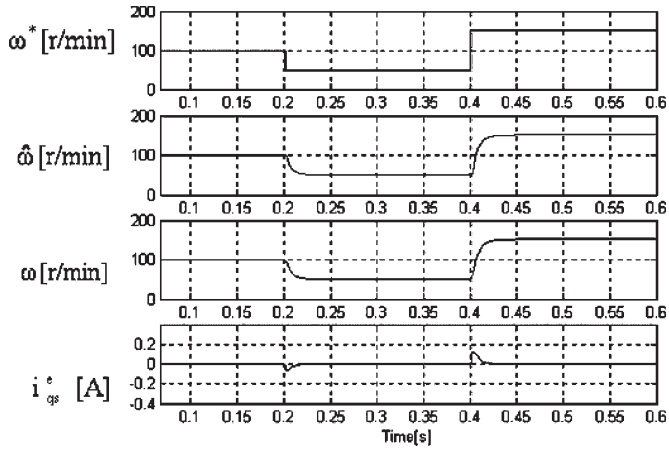


Fig. 9. Estimated and actual rotor speed with step speed command ($100 \rightarrow 50 \rightarrow 150$ r/min).

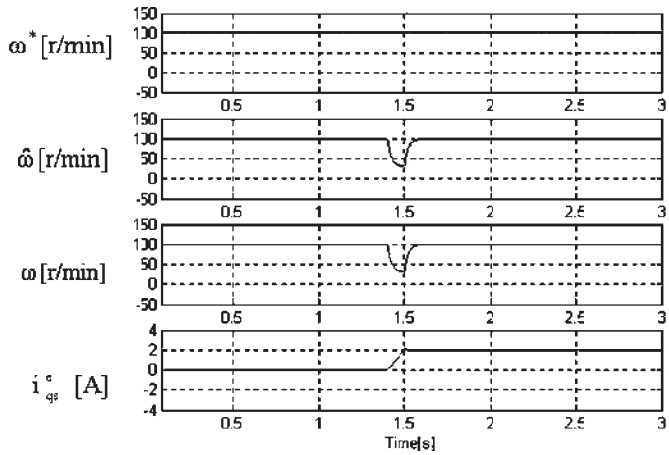


Fig. 10. Responses of the proposed algorithm with 100 r/min speed command under half-rated load condition.

In the proposed sensorless method, the flux linkage of the permanent magnet is only a parameter to estimate the rotor velocity. To examine the parameter sensitivity of the proposed

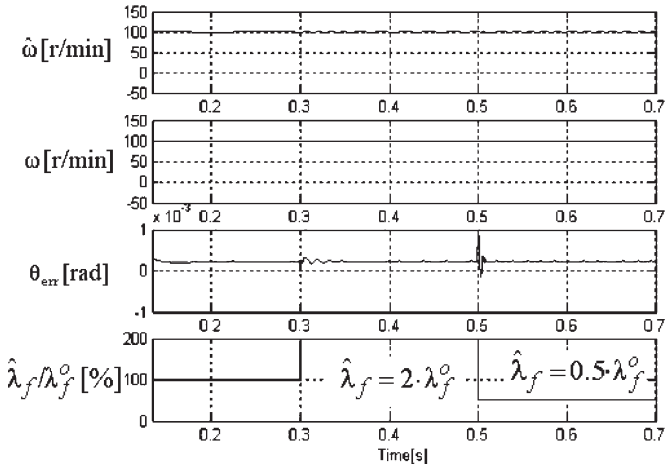


Fig. 11. Sensitivity of the estimation error to parameter variation.

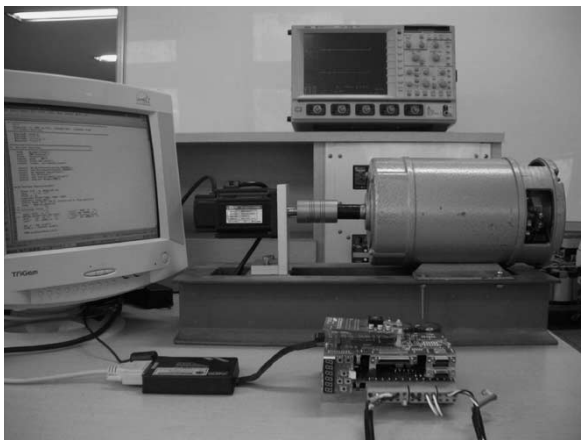

Fig. 12. Experimental setup for load test.

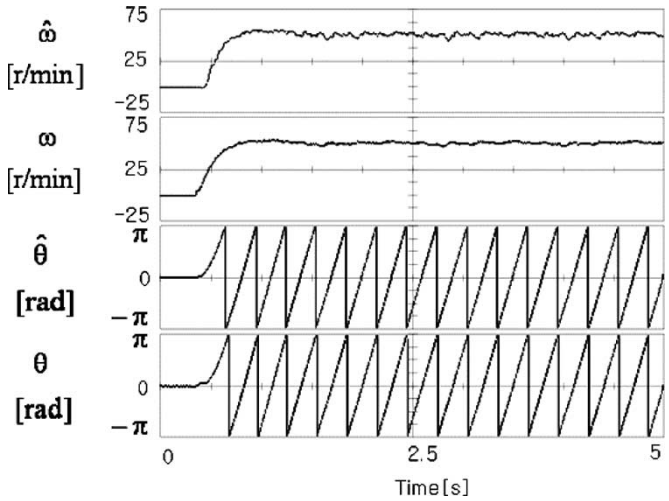


Fig. 13. Estimated and measured speed/position with a step 50-r/min command change.

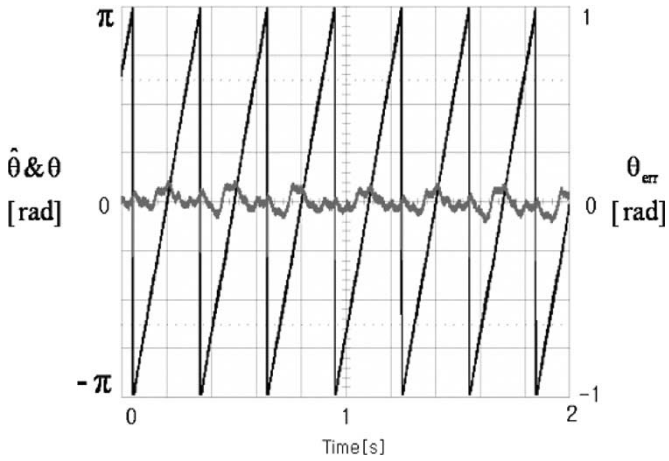


Fig. 14. Responses of position error with 50-r/min speed command.

method, the parameter was intentionally varied stepwise $-50/+100\%$ from its nominal value under 100 r/min speed command as shown in Fig. 11. During this test, the influence of the rotor position error and speed control performance were examined. This variation is thought to be much severer than would be encountered in most practical situations. It is concluded that the amount of the estimated position and speed error is very small enough to achieve robust control against the parameter variation. This feature is mainly due to the employment of a PI-type estimator that is very robust to a modeling error.

## V. Experimental Results

Intensive tests are performed to verify the presented study. The algorithm is programmed and installed to a commercial 600-W PMSM without rotor saliency, which is the same motor that has been used in simulation tests. The PWM VSI inverter consists of 20-kHz switching insulated gate bipolar transistor (IGBT) modules and is controlled by the control board using a digital signal processor (DSP), TMS320VC33 120 MHz. A 750-W dc motor has been coupled with a 600-W PMSM in order to apply the load torque as shown in Fig. 12. Bandwidths of the speed controller and the rotor position tracking PI controller are set to 100 and 300 rad/s, respectively. The phase margin is $50^\circ$ and $K$ is set to 10, which means that control mode switching occurs at 25 r/min. Sampling periods of the current and speed control loops are 50 $\mu$s and 1 ms, respectively.

Fig. 13 shows the estimated and actual speed/position with step speed change from 0 to 50 r/min. From the top, the estimated speed, the measured speed using a 1024 pulse per revolution (p/r) encoder for monitoring, the estimated position, and the measured position are depicted. The test motor has eight poles, so 50 r/min means that the rotor frequency is about 3.3 Hz. It can be seen that the estimated speed is in close agreement with the actual speed under transient state as well as steady state at around zero frequency. From this test, it is worth mentioning that the proposed sensorless PI estimator provides the satisfactory transient performance even at speeds of 3.3 Hz. This improvement is mainly due to the derivation of PI gain formulas based on the frequency-domain analysis and the selection of desired bandwidth considering the effect of a constant $K$.

Fig. 14 shows the performance of the rotor position error in electrical degree with 50-r/min speed command. The rotor position estimation error is confined to nearly zero in steady state.

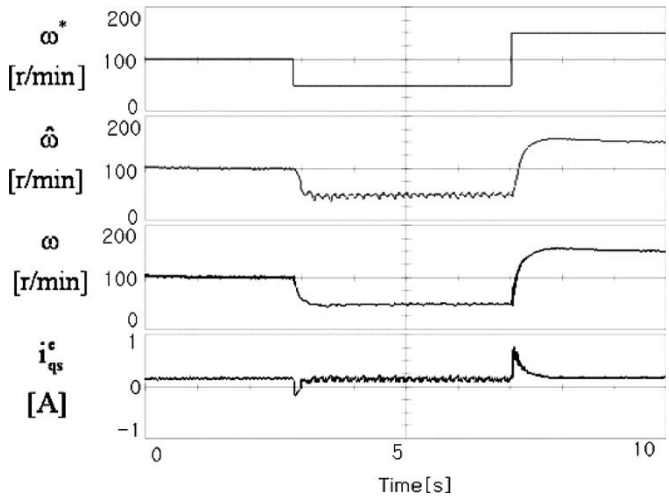


Fig. 15. Responses of estimated and actual rotor speed with varying speed command ($100 \rightarrow 50 \rightarrow 150$ r/min).

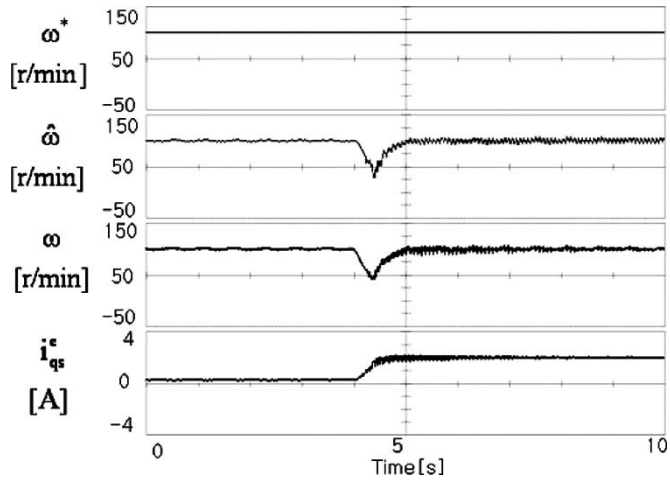


Fig. 16. Responses of the proposed algorithm with 100-r/min speed command under half-rated load condition.

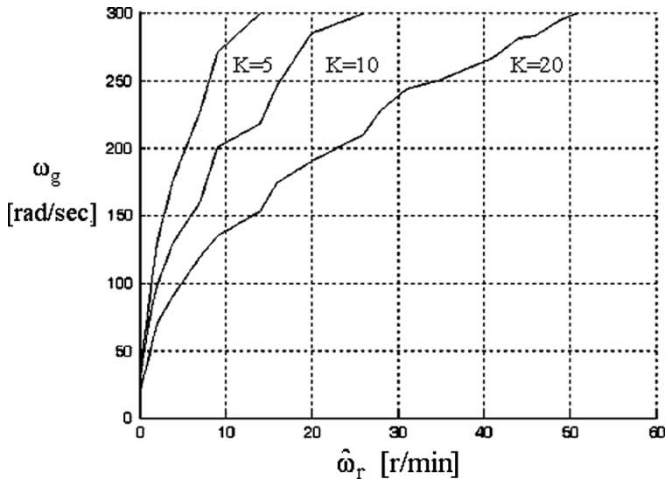


Fig. 17. Experimental bandwidth locus according to estimated rotor velocity.

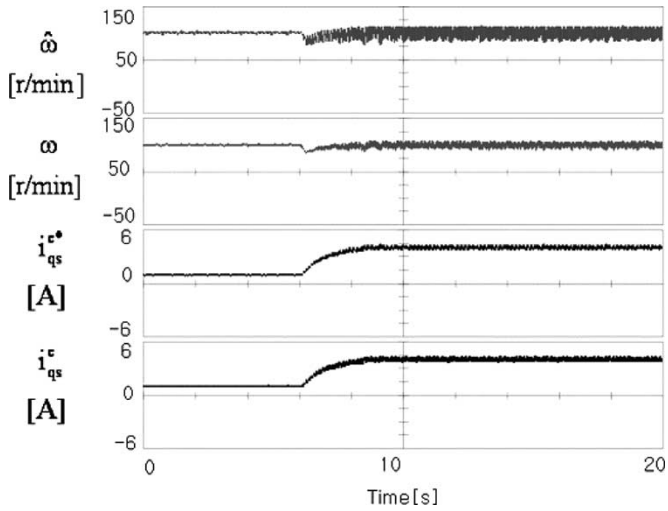


Fig. 18. Transient responses with 100-r/min speed command under rated load condition.

In Fig. 15, the performance of the proposed method is again assessed by changing the speed command from 100 to 50 to 150 r/min. From the top, the speed command, the estimated speed, the actual speed for monitoring, and the $q$-axis current are depicted. At very low speed, the proposed algorithm does not lose the estimation capability under speed transient change and the speed control is stable at transient and steady state.

Fig. 16 shows the response of the proposed sensorless scheme with 100-r/min speed command under the half-rated load condition. This demonstrates that speed estimation and control are robust during a transient load torque change.

Fig. 17 illustrates experimental bandwidth trajectories of the rotor position tracking PI controller according to the estimated velocity. As expected, when $K$ is 10, the sensorless loop gain becomes 300 rad/s at around 30 r/min. From this result, it is concluded that designers can decide the control authority at a given operating frequency before startup.

Fig. 18 shows speed transient responses under load variation from 0 to 1 p.u. when a speed command is set to 100 r/min. From the top, the speed command, the estimated speed, the $q$-axis current command, and the $q$-axis current are depicted. Compared to the no load or half-rated load condition, the speed ripple is somewhat increased, which is mainly caused by dead-time effects, current measurement errors, and mechanical coupling eccentricity. The proposed algorithm does not lose the estimation capability even under the rated load condition. This result shows that the proposed sensorless algorithm yields a satisfactory low-speed control in the vicinity of zero frequency under rated load change.

Fig. 19 shows a plot of the steady-state estimated rotor position and controlled currents under the full-load condition while the motor is running at a constant speed of 100 r/min. As can be seen from heavy load tests, the control performance is very robust in the transient state as well as steady state.

## VI. Conclusion

This paper has described a new back EMF-based sensorless control technique of a nonsalient PMSM. The proposed scheme is based on the $d$-axis current regulator output voltage that has the information of rotor position error. Rotor velocity can be estimated through a rotor position tracking PI controller

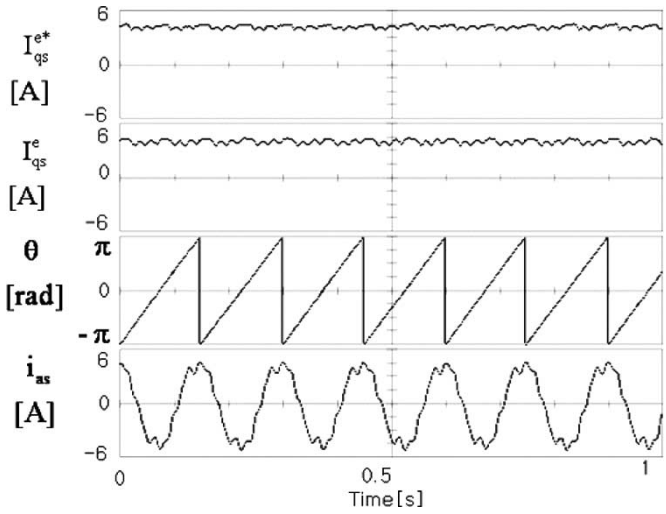


Fig. 19. Steady-state responses with 100-r/min speed command under rated load condition.

that controls the position error to zero. Analyzing this control system by the frequency-domain specification such as phase margin and bandwidth assignment, tuning formulas for the PI controller are derived. The proposed method only requires the flux linkage of the permanent magnet and is insensitive to parameter error and variation.

Designers can easily determine the possible operating range with a desired bandwidth and perform the vector control even at low speeds. The developed algorithm has been implemented on the actual 600-W PMSM drive system. Obtained results confirm the effectiveness of the proposed scheme under heavy load conditions.

## REFERENCES

[1] R. Wu and G. R. Slemon, "A permanent magnet drive without a shaft sensor," *IEEE Trans. Ind. Appl.*, vol. 27, no. 5, pp. 1005–1011, Sep./Oct. 1991.

[2] N. Ertugrul and P. Acarnley, "A new algorithm for sensorless operation of permanent magnet motors," *IEEE Trans. Ind. Appl.*, vol. 30, no. 1, pp. 126–133, Jan./Feb. 1994.

[3] J. S. Kim and S. K. Sul, "New approach for high performance PMSM drives without rotational position sensors," *IEEE Trans. Power Electron.*, vol. 12, no. 5, pp. 904–911, Sep. 1997.

[4] H. Jang, S. K. Sul, J. I. Ha, K. Ide, and M. Sawamura, "Sensorless drive of surface-mounted permanent-magnet motor by high-frequency signal injection based on magnetic saliency," *IEEE Trans. Ind. Appl.*, vol. 39, no. 4, pp. 1031–1039, Jul./Aug. 2003.

[5] B. H. Bae, S. K. Sul, J. H. Kwon, and J. S. Byeon, "Implementation of sensorless vector control for super-high speed PMSM of turbo-compressor," *IEEE Trans. Ind. Appl.*, vol. 39, no. 3, pp. 811–818, May/Jun. 2003.

[6] L. Xu and C. Wang, "Implementation and experimental investigation of sensorless control scheme for PMSM in super-high variable speed operation," in *Conf. Rec. IEEE-IAS Annu. Meeting*, 1998, vol. 1, pp. 483–489.

[7] W. K. Ho, C. C. Hang, and J. H. Zhou, "Performance and gain and phase margins of well-known PI tuning formulas," *IEEE Trans. Contr. Syst. Technol.*, vol. 3, no. 2, pp. 245–248, Jun. 1995.

**Jul-Ki Seok** (S'94–M'98) received the B.S., M.S., and Ph.D. degrees in electrical engineering from Seoul National University, Seoul, Korea, in 1992, 1994, and 1998, respectively.

From 1998 to 2001, he was a Senior Engineer at the Production Engineering Center, Samsung Electronics, Suwon, Korea. Since 2001, he has been with the School of Electrical Engineering, Yeungnam University, Kyongsan, Korea, where he is currently an Assistant Professor. His specific research interests are in high-performance electrical machine drives, control and analysis of linear hybrid stepping motor, and nonlinear system identification as related to the power electronics fields.

**Jong-Kun Lee** (S'04) received the B.S. and M.S. degrees in electrical engineering from Yeungnam University, Kyongsan, Korea, in 2002 and 2005, respectively.

He is with the Robot Institute, Daewoo Ship-Building and Marine Engineering Company Ltd., Geoje City, Korea. His specific research interests are electrical machines, high-performance electrical machine drives, and active power filters.

**Dong-Choon Lee** (S'90–M'95) received the B.S., M.S., and Ph.D. degrees in electrical engineering from Seoul National University, Seoul, Korea, in 1985, 1987, and 1993, respectively.

From 1987 to 1988, he was a Research Engineer at Daewoo Heavy Industry. He also worked at the Research Institute of Science Engineering, Seoul National University, under a Post-Doctoral Fellowship for one year. Since 1994, he has with the Department of Electrical Engineering, Yeungnam University, Kyongsan, Korea. As a Visiting Scholar, he was with the Power Quality Laboratory, Texas A&M University, College Station, in 1998; the Electrical Drive Center, University of Nottingham, U.K., in 2001; and the Wisconsin Electric Machines and Power Electronic Consortium, University of Wisconsin, Madison, in 2004. His research interests include ac machine drives, control of power converters, wind power generation, and power quality.